ADVANCED FUNCTIONAL MATERIALS

FULL PAPER

DOI: 10.1002/adfm.200800633

Organic Phenolic Configurationally Locked Polyene Single Crystals for Electro-optic and Terahertz Wave Applications**

By *O-Pil Kwon,** *Seong-Ji Kwon, Mojca Jazbinsek, Fabian D. J. Brunner, Jung-In Seo, Christoph Hunziker, Arno Schneider, Hoseop Yun, Yoon-Sup Lee,* and *Peter Günter*

We investigate a configurationally locked polyene (CLP) crystal 2-(3-(4-hydroxystyryl)-5,5-dimethylcyclohex-2-enylidene)malononitrile (OH1) containing a phenolic electron donor, which also acts as a hydrogen bond donor. The OH1 crystals with orthorhombic space group $Pna2_1$ (point group mm2) exhibit large second-order nonlinear optical figures of merit, high thermal stability and very favorable crystal growth characteristics. Higher solubility in methanol and a larger temperature difference between the melting temperature and the decomposition temperature of OH1 compared to analogous CLP crystals, are of advantage for solution and melt crystal growth, respectively. Acentric bulk OH1 crystals of large sizes with side lengths of up to 1 cm with excellent optical quality have been successfully grown from methanol solution. The microscopic and macroscopic nonlinearities of the OH1 crystals are investigated theoretically and experimentally. The OH1 crystals exhibit a large macroscopic nonlinearity with four times larger powder second harmonic generation efficiency than that of analogous CLP crystals containing dimethylamino electron donor. A very high potential of OH1 crystals for broadband THz wave emitters in the full frequency range of 0.1–3 THz by optical rectification of 160 fs pulses has been demonstrated.

1. Introduction

Organic nonlinear optical crystals[1,2] have attracted considerable interest for numerous applications, such as optical frequency conversion, integrated photonics[3] and terahertz (THz) wave generation and detection.[4,5] The main requirement for a crystal to show macroscopic second-order nonlinear optical activity is a spontaneous acentric packing of highly polar chromophores, which are highly extended π-conjugated electron donor and acceptor disubstituted molecules. In many acentric crystals, the main supramolecular interactions are weak or strong hydrogen bonds.[6] However, organic nonlinear optical crystals containing phenolic electron donors, which can act as hydrogen bond donor sites, have been rarely investigated.[7,8]

We have recently introduced configurationally locked polyene (CLP) crystals, which are of special interest due to the high tendency for forming acentric crystals with large macroscopic nonlinearity, high thermal stability and the possibility of various melt- and solution-based crystal growth techniques.[9–11] The electron donors in these crystals are various dialkylamino or methoxy groups and the electron acceptor is a dicyanomethylidene, $>C=C(CN)_2$ group, in which the CN group can act as a hydrogen bond acceptor site. The main supramolecular interactions of acentric CLP crystals are hydrogen bonds of –CN. . .HC– or –CN. . .HO– groups.[9–11] The cyano (CN) groups in the electron acceptor form hydrogen bonds with hydrogen bond donor sites in the non-π-conjugated part: for example, H–C groups on the methyl groups in the cyclohexene ring in (2-(3-(2-(4-dimethylaminophenyl)vinyl)-5,5-dimethylcyclohex-2-enylidene)malononitrile (DAT2)[9] and aliphatic H-O group on the prolinol group in 2-(3-(4-(2-(hydroxymethyl)pyrrolidin-1-yl)styryl)-5,5-dimethylcyclohex-2-enylidene)malononitrile (PyM3).[11]

Here we investigate a novel, very promising CLP crystal, OH1 (2-(3-(4-hydroxystyryl)-5,5-dimethylcyclohex-2-enylidene)malononitrile) containing a phenolic electron donor in the π-conjugated part, which also acts as a hydrogen bond donor site. Although the synthesis and the crystal structure of this material have been previously reported,[12,13] its parameters relevant for second-order nonlinear optical applications have not been examined yet. The OH1 chromophores exhibit high

[*] Prof. O-P. Kwon, S.-J. Kwon, Dr. M. Jazbinsek, F. D. J. Brunner, C. Hunziker, Dr. A. Schneider, Prof. P. Günter
Nonlinear Optics Laboratory, ETH Zurich
8093 Zurich (Switzerland)
E-mail: nlo@phys.ethz.ch
Prof. O-P. Kwon
Department of Molecular Science and Technology, Ajou University
Suwon 443-749 (Korea)
E-mail: opilkwon@ajou.ac.kr
J.-I. Seo, Prof. Y.-S. Lee
Department of Chemistry and School of Molecular Science (BK 21)
Korea Advanced Institute of Science and Technology (KAIST)
Daejeon 305-701 (Korea)
Prof. H. Yun
Division of Energy Systems Research and Department of Chemistry, Ajou University
Suwon 443-749 (Korea)

[**] We thank J. Hajfler for the polishing of OH1 samples. This work has been supported by the Swiss National Science Foundation and the Korea Foundation for International Cooperation of Science & Technology (KICOS) through a grant provided by the Korean Ministry of Science & Technology(MOST) (No. 2007-00440).

ADVANCED FUNCTIONAL MATERIALS

thermal stability and high solubility in methanol that leads to relatively easy growth of high optical quality large size OH1 crystals from methanol. The microscopic and macroscopic nonlinearities of the OH1 crystals are investigated experimentally and theoretically by using the time-dependent density functional theory (TD-DFT) and finite field (FF) methods. Highly efficient second-harmonic generation at 1907 nm fundamental wavelength and THz wave generation using 160 fs pump pulses at 1460 nm in OH1 crystals has been demonstrated.

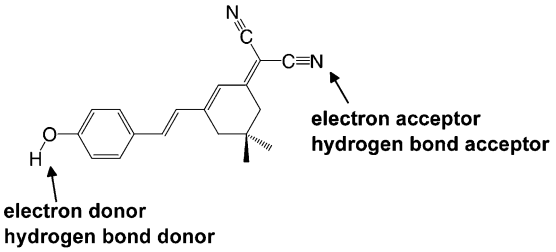

Scheme 1. The chemical structure of the investigated OH1 chromophore with phenolic electron and hydrogen bond donor.

2. Results and Discussion

2.1. Synthesis and Characterization

The chemical structure of the OH1 chromophore investigated is shown in Scheme 1. The OH1 chromophore consists of the configurationally locked π-conjugated hexatriene bridge linked between phenolic electron donor and dicyanomethylidene [>C=C(CN)$_2$] electron acceptor, which can also act as hydrogen bond donor and acceptor site, respectively. The OH1 chromophore was synthesized by consecutive Knoevenagel condensations.[12–14] For introducing phenolic electron and hydrogen bond donor sites 4-hydroxybenzaldehyde was used for the synthesis. In order to retain high thermal stability and the tendency for inducing an acentric packing,[9] structurally asymmetric groups were incorporated in the cyclohexene ring of the OH1 chromophore as demonstrated in some previously studied CLP crystals.[9–11] The product was purified several times by recrystallization in methanol.

The results of the physical characteristics, including the thermal properties, absorption properties, macroscopic nonlinearity and crystal properties of OH1 crystals are summarized in Table 1 and compared to the analogue polyene DAT2 crystal[9] and the state-of-the-art organic nonlinear optical crystal salt DAST (*N*,*N*-dimethylamino-*N*′-methylstilbazolium *p*-toluenesulfonate).[15]

Figure 1 shows the absorption spectra of OH1 molecules in various polar and nonpolar solvents. The wavelength of the maximum absorption λ_{max} is considerably shifted depending on the environmental conditions (i.e., on the different solvents): 427 nm in THF, 426 nm in methanol, 423 nm in chloroform, 417 nm in acetonitrile, and 415 nm in dioxane. This can be attributed to intermolecular hydrogen bond formation between the phenolic group of the OH1 molecule and the solvent.[16] This binding is affecting the electron donating strength and results in a change of the wavelength of maximum absorption λ_{max}.

The thermal stability of the OH1 chromophore was investigated using thermogravimetric analysis (TGA) and differential scanning calorimetry (DSC) under nitrogen atmosphere (scan rate: 10 °C min^{-1}). The melting temperature T_m is defined here as the peak position in the DSC scan. The thermal weight-loss temperature T_i was estimated as the temperature at the intercept of the leading edge of the weight loss by the base line of the TGA scans. The OH1 chromophore exhibits a very high weight-loss temperature T_i of 325 °C, which involves sublimation and/or decomposition. The OH1 crystals exhibit a large temperature difference ΔT of about 113 °C between the

Table 1. Comparison of crystal properties for the OH1 crystals, analogous DAT2 crystals, and the state-of-the-art organic nonlinear optical crystal salt DAST. Powder SHG measured at a fundamental wavelength of 1.9 μm relative to that of DAT2 powder (about two orders of magnitude larger than that of urea).

	OH1	DAT2	DAST
wavelength of maximal absorption λ_{max} (nm)	423 (chloroform)	502 (chloroform)	475 (methanol)
crystal system space group (point group)	orthorhombic $Pna2_1$ ($mm2$)	monoclinic $P2_1$ (2)	monoclinic Cc (m)
polar axis	*c*-axis	*b*-axis	*a*-axis
usual habit	*a*-plate	*c*-plate	*c*-plate
crystal quality: spontaneous growth in solution	excellent	good	good
solubility at 40 °C (g/100 g methanol)	3.74	<0.01	3.73
bulk crystal growth	easy	difficult	moderate
polymorph	no	no	centrosymmetric hydrate
thermal weight-loss temperature T_i	325 °C	293 °C	250 °C
melting temperature T_m	212 °C	233 °C	250 °C ($\approx T_i$)
possibility for melt-based growth ($\Delta T = T_i - T_m$)	possible ($\Delta T = 113$ °C)	possible ($\Delta T = 60$ °C)	very difficult ($\Delta T \approx 0$ °C)
powder SHG at 1.9 μm	4	1	8
electro-optic coefficient	$r_{333} = 52$ pm V^{-1} at 1.3 μm	–	$r_{111} = 53$ pm V^{-1} at 1.3 μm
cut-off wavelength	<640 nm	–	< 680 nm
solubility in water	insoluble	insoluble	soluble

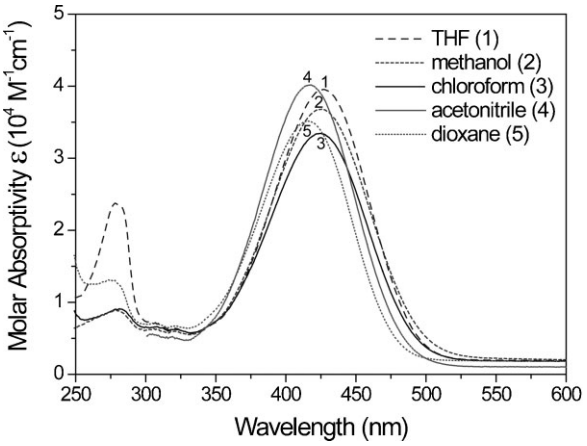

Figure 1. Absorption spectra of OH1 molecule in different solvents: THF (1, $\lambda_{max} = 427$ nm), methanol (2, $\lambda_{max} = 426$ nm), chloroform (3, $\lambda_{max} = 423$ nm), acetonitrile (4, $\lambda_{max} = 417$ nm), and dioxane (5, $\lambda_{max} = 415$ nm).

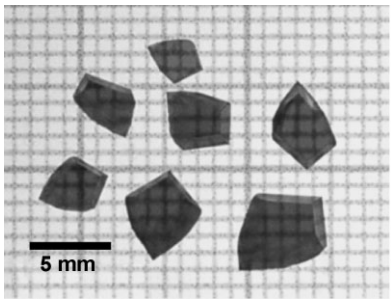

Figure 2. Bulk OH1 crystals grown in methanol solution by the slow evaporation method.

thermal weight-loss temperature T_i and the melting temperature T_m. The high thermal stability of OH1 crystals is an advantage for applying a melt-based crystal growth that is difficult for the ionic salts, e.g., DAST that decomposes at the melting temperature.

2.2. Large Size Single Crystals

CLP crystals studied previously are soluble in polar solvents such as acetone, acetonitrile and dimethylformamide and in a nonpolar solvent methylenechloride, while the solubility in methanol or ethanol is too low for growing bulk crystals.[9] Due to the highly polar phenolic OH group, the OH1 crystals are well dissolved in methanol, compared to, e.g., DAT2 crystals that have a dimethylamino group and exhibit poor solubility as listed in Table 1. The higher solubility of OH1 crystals is of advantage for solution growth because of a better material transport leading to faster growth rates and/or larger crystal dimensions.

We grew easily large size bulk OH1 crystals by slow evaporation in methanol solution at 30 °C. We did not observe any hydrated phase of OH1 crystal during the crystal growing process. The growth procedure was very simple and the growth process has not been optimized yet. In the beginning, several crystals nucleated at the bottom of an open glass container and then continued to grow during 10 days. Figure 2 shows a photograph of the resulting OH1 single crystals. As-grown OH1 crystals exhibit excellent optical quality and large size with a maximal side length of up to 1 cm. The thickness of the crystals is in the range of 0.1–2 mm. The grown OH1 crystals are of sufficient size and thickness for nonlinear optical experiments including THz wave generation. Moreover, non-ionic type OH1 crystals are insoluble in water, in contrast to highly soluble ionic DAST crystals, which easily form a centrosymmetric hydrated phase with water. Therefore, OH1 crystals possess better environmental stability, and allow for wet structuring processes. After growing, the larger surfaces of the crystals were polished to $\lambda/4$ surface quality for optical characterization.

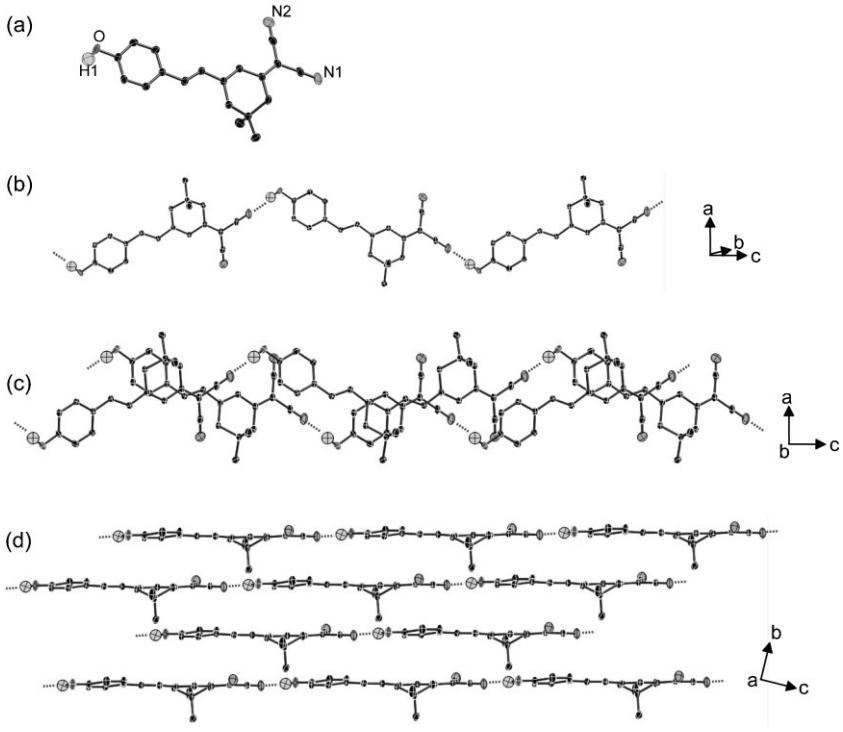

Figure 3. a) Molecular structure of the OH1 chromophore in the crystalline state. Acentric polymer-like chains: top view of an acentric chain (b), top (c), and side (d) view of a stack of acentric chains. Hydrogen atoms excluding those on OH group are omitted for clarity. OH1 molecules in the acentric chain are linked with hydrogen bonds of C≡N...H-O with N...H distances of about 2.12 Å, which are indicated by dotted lines.

ADVANCED FUNCTIONAL MATERIALS

2.3. Crystal Structure

The crystal structure of OH1 grown from methanol solution was determined by X-ray diffraction in order to compare it with the previously published crystal structure of OH1 grown from ethyl acetate solution.[13] The OH1 crystals grown from methanol solution exhibit practically identical crystal structure as those grown from ethyl acetate solution, i.e., polymorphism was not observed. The OH1 crystals have a noncentrosymmetric structure, orthorombic with space group symmetry $Pna2_1$ and point group symmetry $mm2$. The molecular structure and crystal packing diagrams of the OH1 chromophores are shown in Figures 3–5.

As in previously studied PyM3 crystals[11] containing aliphatic hydroxyl OH groups, the main supramolecular interactions of the OH1 crystals are strong hydrogen bonds of C=N...H–O (see Figs. 3 and 4). For both OH1 and PyM3 crystals, the hydrogen bond acceptor site corresponds to the nitrogen atom (N1) on the electron acceptor group. However, for OH1 crystals the hydrogen bond donor site corresponds to the phenolic hydroxyl group in the π-conjugated part, while for PyM3 crystals it corresponds to the aliphatic hydroxyl group in the non-π-conjugated part. As shown in Figure 3b, the nitrogen atom (N1) on the CN group and the hydrogen atom on the phenolic OH group are linked by a strong hydrogen bond with a H...N distance of about 2.12 Å. With the help of these two hydrogen bonding sites at opposite ends, nearly planar OH1 molecules build a hydrogen-bonded polar polymer-like chain in the crystalline solid. The polar polymer-like chains are stacked up one by one, forming acentric layers as shown in Figure 3c and d. The polar direction of the acentric layers makes an angle of about 20° with the polar crystallographic c axis in the bc plane (see Figs. 4 and 5).

OH1 crystals feature a relatively high point-group symmetry compared to other organic crystals. They belong to the orthorhombic crystal system, for that the dielectric axes coincide with the crystallographic axes. This is of advantage since it allows a much simpler crystal preparation and orientation for optical characterization and applications. Most of the known highly nonlinear optical crystals feature lower crystal symmetry, typically crystallizing in monoclinic crystal

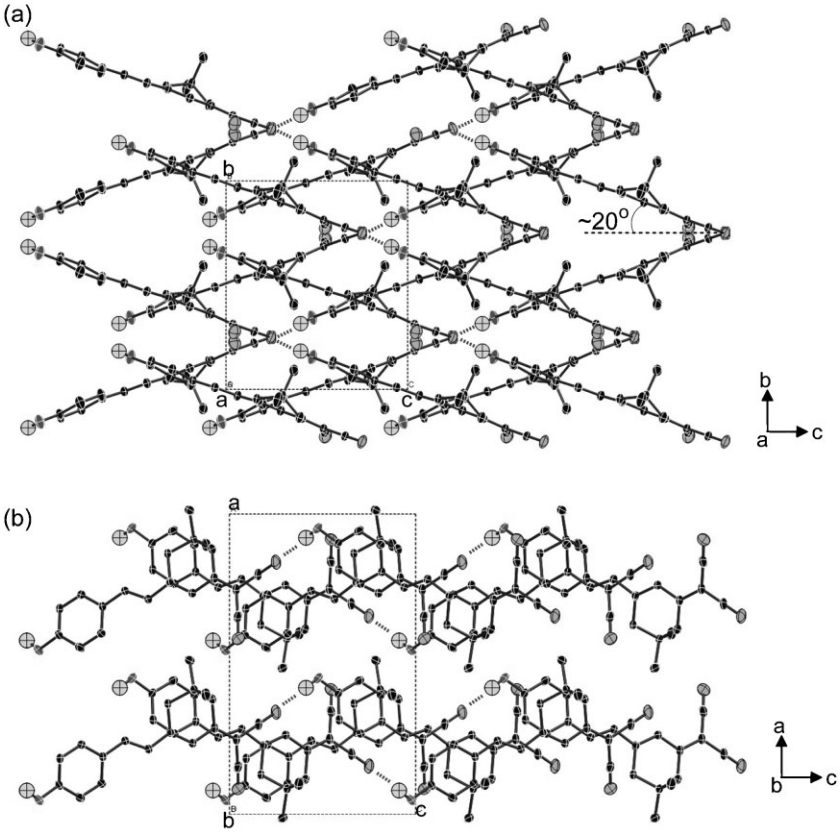

Figure 4. The relative arrangement of both acentric layers in OH1 projected along the *a*-axis (a) and along the *b*-axis (b). Hydrogen atoms excluding those on OH group are omitted for clarity.

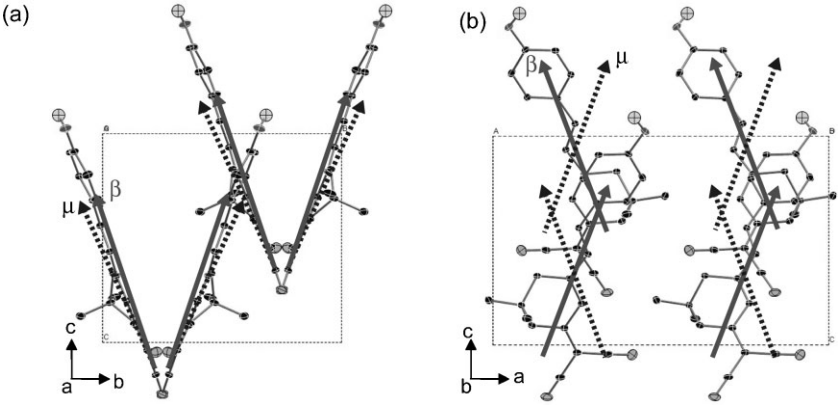

Figure 5. Crystal packing diagram of OH1 crystal projected along the *a*-axis (a) and along the *b*-axis (b). The solid and dotted vectors present the directions of the maximum first hyperpolarizability β_{max} and the dipole moment μ of four OH1 molecules in the unit cell as determined by finite-field calculations, respectively. Hydrogen atoms excluding those on OH group are omitted for clarity.

systems: for example DAT2,[9] PyM3,[11] DAST,[15] DAPSH,[17] and Mero-2-MDB.[8]

2.4. Linear Optical Properties

The transmission spectra of a polished OH1 crystal (*a*-plate) with a thickness of 1.44 mm was measured for the incident light polarized parallel to the crystallographic *b*- and *c*-axis and is shown in Figure 6. OH1 crystals exhibit a large transparency range from 700 to 1400 nm. Three absorption bands observed in the infrared region at about 1.5, 1.7, and 1.8 μm correspond to overtones of the O–H and C–H stretching vibrations. The absorption edge is shifted to shorter wavelength by about 40 nm with respect to the one in DAST.[15] The larger transparency range in the visible and the lower cut-off wavelength of OH1 crystals can be used for applications in the red and near-IR wavelength range and may also lead to a better photostability.[18]

2.5. Microscopic and Macroscopic Optical Nonlinearities in the Crystallographic System

The macroscopic second-order susceptibilities $\chi^{(2)}$ can be estimated from the microscopic first hyperpolarizabilities β_{ijk} using the oriented gas model, giving, e.g., for second-harmonic generation[1]

$$\chi^{(2)}_{ijk}(-2\omega,\omega,\omega) = Nf_i^{2\omega}f_j^{\omega}f_k^{\omega}\beta^{\mathrm{eff}}_{ijk}(-2\omega,\omega,\omega), \quad (1)$$

where N is the number of molecules per unit volume and f_i^{ω} are the local filed correction factors. The effective $\beta^{\mathrm{eff}}_{ijk}$ coefficients in the crystal can be calculated from the hyperpolarizability tensor components β_{mnp} of the molecules as

$$\beta^{\mathrm{eff}}_{ijk} = \frac{1}{n(g)}\sum_{s}^{n(g)}\sum_{mnp}^{3}\cos(\theta^s_{im})\ \cos(\theta^s_{jn})\cos(\theta^s_{kp})\,\beta_{mnp}, \quad (2)$$

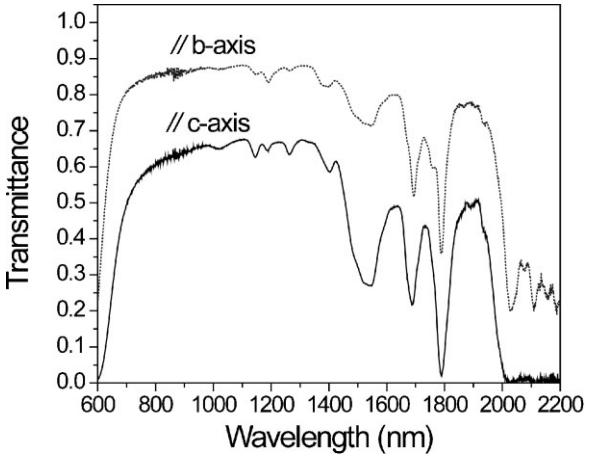

Figure 6. Transmission spectra of a polished OH1 crystal (*a*-plate) with a thickness of 1.44 mm for the incident light polarized parallel to the crystallographic *b*- and the polar *c*-axis.

where $n(g)$ is the number of equivalent positions in the unit cell, s denotes a site in the unit cell, and $\theta_{im}{}^{s}$ is the angle between the Cartesian axis i and the molecular axis m.

The first hyperpolarizability β was determined experimentally by electric field induced second harmonic generation measurements (EFISH) at the wavelength 1907 nm and theoretically by quantum chemical calculations. For the theoretical calculations, the molecular geometries were fully optimized without restrictions using the hybrid functional B3LYP[19] with the 6-311+G(d) basis set. The optimized (OPT) molecules, calculated by the Gaussian 03 program,[20] and experimental (EXP) molecules, determined by the X-ray diffraction analysis, were analyzed by finite field (FF) and time-dependent density functional theory (TD-DFT) methods. The results of the calculated hyperpolarizabilities are given in Tables 2, 3, and their comparison to the experimentally determined values in Table 4. The optimized (OPT) and experimental (EXP) molecules show similar microscopic molecular nonlinearities in the quantum chemical calculations. As listed in Table 4, the molecular hyperpolarizability β_z measured by EFISH for the OH1 chromophore varies considerably in different solvents, chloroform and dioxane. We attribute this difference to different intermolecular interactions between the OH1 molecules and the solvent molecules, inducing a change of the electron donating strength, changing also the wavelength of maximum absorption $\lambda_{\max}$.

As listed in Table 2 and illustrated in Figure 5, the OH1 molecules in the crystalline state have a large angle of about 42° between the direction of the maximum first hyperpolarizability $\beta_{\max}$ and the dipole moment μ. The direction of the maximum first hyperpolarizability $\beta_{\max}$ of the OH1 molecules is aligned at a small angle of $\theta_p = 28°$ with the polar *c*-axis. We

Table 2. Results of the finite-field (FF) method calculated with the optimized (OPT) and experimental (EXP) molecular structures: dipole moments μ_g (D), the zero-frequency hyperpolarizability tensor β_{ijk} ($\times 10^{-40}$ m^4 V^{-1}), the vector component β_z ($\times 10^{-40}$ m^4 V^{-1}) along the dipole moment direction of the hyperpolarizability tensor β_{ijk}, the first hyperpolarizability $\beta_{\max}$ ($\times 10^{-40}$ m^4 V^{-1}), and the angle θ (deg.) between the dipole moment μ_g and the main direction of the first hyperpolarizability $\beta_{\max}$. The *z*-direction is the direction of the ground-state dipole moment μ_g. 1×10^{-40} m^4 V^{-1} corresponds to 0.239×10^{-30} esu is the cgs unit system.

	OH1 (OPT)	OH1 (EXP)	DAT2 (OPT)	DAT2 (EXP)
μ_g (=$-\mu_z$)	11.39	10.96	14.01	13.72
β_{xxx}	−1.0	−0.3	−1.1	−0.2
β_{xxy}	−1.7	−1.0	−0.5	−0.1
β_{xyy}	−7.8	−6.4	−3.2	−0.4
β_{yyy}	−102	−102	−44	−57
β_{xxz}	−1.3	−1.6	−4.2	−3.9
β_{xyz}	11.4	8.0	10.8	2.5
β_{yyz}	140	129	134	150
β_{xzz}	−13.6	−9.6	−27	−7.9
β_{yzz}	−171	−149	−337	−345
β_{zzz}	177	151	698	690
β_z	316	280	827	836
β_{max}	434	388	942	950
θ	40.4	41.6	24.5	25.5

ADVANCED FUNCTIONAL MATERIALS

Table 3. Results of TD-DFT calculation from the optimized (OPT) and experimental (EXP) molecular structures using B3LYP/6-311+G(d).

	OH1 (OPT)	OH1 (EXP)	MM1 (OPT)	MM1 (EXP)
Major contribution	HOMO-1 → LUMO (2.5%) HOMO → LUMO (74.8%)	HOMO-1 → LUMO (2.5%) HOMO → LUMO (73.4%)	HOMO-1 → LUMO (2.3%) HOMO → LUMO (75.2%)	HOMO → LUMO (77.3%)
λ_{max} (nm)	415	395	468	463
E_{max}[ICT] (eV)	2.99	3.14	2.65	2.68
f_{os}	1.30	1.33	1.30	1.20
μ_{ge} (D)	10.71	10.55	11.40	10.85
$\Delta\mu_{ge}$ (D)	11.72	12.13	17.61	19.58
β_0 (10^{-40} m^4 V^{-1})	368	335	800	788

therefore expect a large macroscopic nonlinearity of OH1 crystals. The Kurtz and Perry powder test[21] was performed at the fundamental wavelength of 1.9 μm. We compared the second harmonic generation (SHG) signal with the signal generated by the DAT2 crystalline powder, which possesses two orders of magnitude greater SHG efficiency than urea.[9] OH1 crystals exhibit very strong SHG signal that is about 4 times larger than the one of DAT2, despite of the lower microscopic molecular nonlinearity (see Tables 2–4).

The reason for the about four times higher SHG efficiency of the OH1 crystals compared to the analogous DAT2 crystals can be related to the ordering of the chromophores in the crystalline lattice.[1] The effective β_{ijk}^{eff} coefficients were calculated from the hyperpolarizability tensor components β_{mnp} using Equation 2 and the results are given in Table 5. The maximum diagonal coefficient β_{iii}^{eff} can be estimated as $\beta_{max}\cos^3\theta_p$. For DAT2 the angle θ_p between the main direction of the first hyperpolarizability and the polar axis was quite large (82°) and for MH2 with the highest powder SHG efficiency it was still 67°.[10] Therefore, the order parameter $\cos^3\theta_p$ is considerably improved in OH1 crystals and this is the first CLP crystal with a highly polar alignment of the chromophores. As listed in Table 5, the maximal component of the effective hyperpolarizability tensor $\beta_{ijk}^{eff} \propto \chi_{ijk}^{(2)}$ is by a factor of about two larger in OH1 compared to DAT2. Therefore, larger components of β_{ijk}^{eff} lead to a considerably higher SHG efficiency of OH1 crystals.

The electro-optic coefficients listed in Table 1 were measured by the phase modulation technique, details will be reported elsewhere.[22] We obtained the electro-optic coefficient of $r_{333} = (52 \pm 7)$ pm V^{-1} at 1.3 μm, which is similar as that of the state-of-the-art organic nonlinear optical crystal salt DAST, with the largest coefficient of $r_{111} = (53 \pm 6)$ pm V^{-1} at 1.3 μm.[15]

Table 4. Hyperpolarizabilities β_z and dipole moments μ_g for OH1 and DAT2 molecules.

	environmental condition	λ_{max} (nm)	μ_g (10^{-29}C m)	β_z (10^{-40} m^4 V^{-1})
OH1	chloroform	423[a]	3.44[a]	765[a]
	dioxane	415[a]	2.20[a]	375[a]
	OPT (cal.)	415[b]	3.80[c]	314[c]
	EXP (cal.)	395[b]	3.65[c]	279[c]
DAT2	chloroform	502[a]	3.21[a]	1100[a]
	OPT (cal.)	468[b]	4.67[c]	825[c]
	EXP (cal.)	463[b]	4.57[c]	834[c]

[a] From the measurements. [b] From TD-DFT calculation. [c] From FF calculation.

2.6. Terahertz Generation

Terahertz time-domain spectroscopy is a powerful technique for an increasing number of applications.[4] It relies on few-cycle pulses of electromagnetic radiation with a spectral content in the 0.1 to 5 THz range that can be generated through optical rectification of sub-picosecond pump laser pulses in second-order nonlinear optical materials. Organic crystals such as DAST have been demonstrated to be very efficient emitters of terahertz pulses.[5] We have generated few-cycle terahertz pulses in single crystals of OH1 and compared them to pulses from DAST under identical experimental conditions. The 160 fs pump laser pulses stem from an optical parametric amplifier pumped by an amplified Ti:Sapphire laser. We chose a central wavelength of 1460 nm for the pump pulses to ensure phase-matched optical rectification in DAST. The terahertz pulses were coherently detected through electro-optic sampling in a ZnTe crystal using probe pulses at 730 nm.[5]

Figure 7 shows a quasi single-cycle terahertz pulse emitted from OH1. Its peak amplitude (at $t = 0$) exceeds that from DAST by 38% despite the shorter crystal length (OH1: 0.365 mm, DAST: 0.400 mm). The terahertz pulse energy from OH1 – proportional to the time integral of the square of the amplitude in Figure 7a – was 8% larger than that from DAST. A significant difference between the two emitter materials is observed in the frequency spectra of their time-domain waveforms as shown in Figure 7b. DAST suffers from a phonon resonance centered at 1.1 THz that leads to an

Table 5. The calculated components of the non-resonant effective hyperpolarizability tensor β_{ijk}^{eff} (10^{-40} m^4 V^{-1}) for OH1 and DAT2 in the dielectric system.

OH1	β_{113}^{eff}	β_{223}^{eff}	β_{333}^{eff}	
	36	30	265	
DAT2	β_{112}^{eff}	β_{222}^{eff}	β_{332}^{eff}	β_{123}^{eff}
	−134	3.9	2.1	0

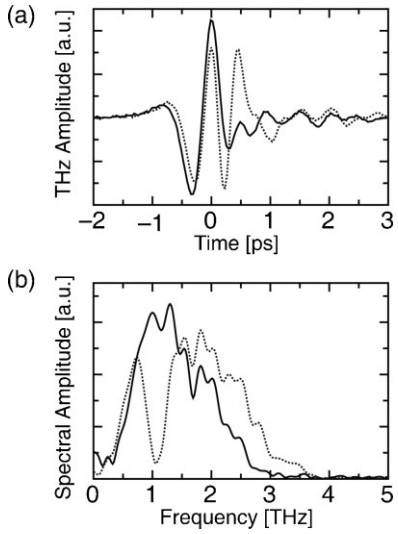

Figure 7. Few-cycle terahertz pulses generated in single crystals of OH1 (thickness 0.365 mm, solid line) and DAST (thickness 0.400 mm, dotted line) at a laser wavelength of 1460 nm. a) Time-domain waveforms of the terahertz electric field E(t). b) Their frequency spectra $E(\nu)$.

increased absorption and consequently to a drastically lower amplitude emitted at this frequency.[23] Apparently, there is no such resonance in OH1 which leads to a relatively smooth spectrum from 0.1 to 3 THz. However, DAST provides a better amplitude at higher frequencies (>1.7 THz). These results demonstrate that OH1 has a very high potential as a source of terahertz radiation, especially considering that these measurements were done with a pump wavelength that is optimized for DAST and not for OH1. The efficiency of terahertz generation from OH1 may still be improved using the proper phase-matching conditions that are currently a subject under investigation.

3. Conclusions

We present a novel CLP crystal OH1 (2-(3-(4-Hydroxystyryl)-5,5-dimethylcyclohex-2-enylidene)malononitrile) containing a phenolic electron donor, which also acts as a hydrogen bond donor site. The OH1 crystals with orthorhombic space group $Pna2_1$ exhibit high second-order nonlinear optical activity, high thermal stability and favorable crystal growth characteristics. The OH1 crystals possesses higher solubility in methanol and reveal a larger temperature difference between the melting temperature and the decomposition temperature compared to analogous CLP crystals, which are of advantage for solution and melt crystal growth, respectively. Acentric bulk OH1 crystals of large sizes with a maximal side length of up to 1 cm with excellent optical quality were successfully grown from methanol solution. The microscopic and macroscopic nonlinearities of the OH1 crystals are investigated theoretically and experimentally. The OH1 crystals exhibit a large macroscopic nonlinearity with four times larger powder second-harmonic generation (SHG) efficiency than analogous CLP crystals containing dimethylamino electron donors. Highly efficient generation of broadband THz waves in the range of 0.1–3 THz using OH1 single crystals has been demonstrated.

4. Experimental

Synthesis of OH1: The 2-(3-(4-hydroxystyryl)-5,5-dimethylcyclohex-2-enylidene)malononitrile (OH1) chromophore was synthesized by Knoevenagel condensations according to literature [9,12–14]. 4-Hydroxybenzaldehyde (17.6 g, 144 mmol) and the intermediates 2-(3,5,5-trimethylcyclohex-2-enylidene)malononitrile (24.8 g, 144 mmol) were dissolved in ethanol (500 mL). Piperidine (144 mmol) was added to this solution and the mixture was stirred for 24 h at room temperature. The resulting mixture was concentrated and subsequently separated by column chromatography (methylene chloride: methanol = 300:1). The product was purified several times by recrystallization in methanol (yield 30%). The chemical shifts in ^{1}H NMR spectra (Varian 300 MHz NMR spectrometer) are reported in ppm (δ) relative to $(CH_3)_4Si$. ^{1}H NMR (300 MHz, CD_3OD, δ): 1.07 (s, 6H,–CH_3), 2.55 (s, 2H, –CH_2–), 2.61 (s, 2H, –CH_2–), 6.78 (s, 1H, –C=CH–), 6.68–6.81 (d, $J = 8.7$ Hz, 2H, Ar–H), 6.95–7.01 (d, $J = 18$ Hz, 1H, –CH=CH–), 7.15–7.21 (d, $J = 18$ Hz, 1H, –CH=CH–), 7.46–7.49 (d, $J = 8.7$ Hz, 2H, Ar–H). Anal. calcd for $C_{19}H_{18}N_2O$: C 78.59, H 6.25, N 9.65, O 5.51; found C 78.47, H 6.44, N 9.63.

Crystal Structure Data for the OH1 Crystal: $C_{19}H_{18}N_2O$, $M_r = 290.37$, orthorhombic, space group $Pna2_1$, $a = 15.4408(6)$ Å, $b = 10.9939(3)$ Å, $c = 9.5709(3)$ Å, $\alpha = 90°$, $\beta = 90°$, $\gamma = 90°$, $V = 1624.70(9)$ Å^3, $Z = 4$, $T = 293(2)$ K, CCDC 672263, μ(Mo Kα) = 0.072 mm^{-1}. Of 15147 reflections collected in the θ range 2.0–27.5° using ω scans on a Rigaku R-axis Rapid S diffractometer, 3552 were unique reflections ($R_{int} = 0.0164$,completeness = 99.7%). The structure was solved and refined against F^2 using SHELX97 [24], 271 variables, $wR2 = 0.0947$, $R1 = 0.0343$ (3120 reflections having $F_o^2 > 2\sigma(F_o^2)$), GOF = 1.076, and max/min residual electron density 0.128/–0.181 eÅ^{-3}.

Powder SHG Measurements: A tunable output of an optical parametric amplifier pumped by an amplified Ti:sapphire laser was used for the Kurtz and Perry powder test [21]. Experiments at a fundamental wavelength of 1.9 μm were done with the parametric signal wave. After grinding OH1 materials, the crystalline powder was put into a 1.00 mm Hellma UV quartz cell to give a constant sample thickness. The backscattered light at the second-harmonic wavelength (953.5 nm) was measured with a silicon photodiode.

EFISH Experiments: For the measurements of the $\mu_g\beta_z$ values, electric field induced second harmonic generation measurements (EFISH) were performed as described in Reference [9a, 25], with pulses at the wavelength 1907 nm that were generated by focusing light of a Q-switched Nd:YAG laser ($\lambda = 1064$ nm, repetition rate 10 Hz, pulse duration 25 ns) into a Raman cell filled with 25 bar H_2. Voltage pulses of 30 μs durations were applied to the wedged cell, generating a static field of around 11 kV cm^{-1}. As reference a 1% MNA dioxane solution was used with a macroscopic third-order nonlinearity $\Gamma = 9.14 \times 10^{-22}$ m^2 V^{-2} [14], which was measured with a quartz reference having a second-order nonlinear optical coefficient $d_{11} = 0.277$ pm V^{-1} [25, 26]. All measurements were performed with chloroform and dioxane as solvent.

Computational Details: To determine molecular nonlinearity in the crystalline state, quantum chemical calculations were performed using Gaussian 03 Program [20] in the same manner as in Ref. [10]. The molecular geometries were fully optimized with no restrictions by using the hybrid functional B3LYP [19] with the 6-311+G(d) basis set. Using the finite-field (FF) method, the hyperpolarizability tensor β_{ijk} was calculated in the molecular system xyz, which is here defined so that the direction of the ground-state dipole moment μ_g points along its

ADVANCED FUNCTIONAL MATERIALS

z direction ($\mu_g = -\mu_z$). The components of the hyperpolarizability tensor β_{ijk} in this system are given in Table 2. We have also determined the main direction and the main value β_{max} of the first hyperpolarizability, which are given in Table 2 as well.

By the electric-field-induced second-harmonic generation (EFISH) experiments only the vector component along the dipole moment μ_g direction is measured. The vector part β_z of the hyperpolarizability tensor β_{ijk} is calculated as

$$\beta_z = \beta_{zzz} + \beta_{xxz} + \beta_{yyz} \quad (3)$$

and is reported in Table 2 as well.

For the TD-DFT calculation, the two-level model was used [27], in which the static first hyperpolarizability β_0 is given by

$$\beta_0 = \frac{3\Delta\mu_{ge}(\mu_{ge})^2}{2(E_{max})^2} \quad (4)$$

where μ_{ge} is the transition dipole moment between the excited and the ground state, $\Delta\mu_{ge}$ is the dipole moment change, and E_{max} is the energy of the maximal charge transfer absorption. The results of TD-DFT calculation from the optimized (OPT) and experimental (EXP) molecular structures are given in Table 3.

Received: May 7, 2008
Published online: September 29, 2008

[1] a) M. Jazbinsek, O. P. Kwon, C. Bosshard, P. Günter, in *Handbook of Organic Electronics and Photonics*, (Ed: S. H. Nalwa), American Scientific Publishers, Los Angeles **2008**, Ch. 1. b) C. Bosshard, M. Bösch, I. Liakatas, M. Jäger, P. Günter, in *Nonlinear Optical Effects and Materials*, (Ed: P. Günter), Springer, Berlin **2000**, Ch. 3. c) C. Bosshard, K. Sutter, P. Prêtre, J. Hulliger, M. Flörsheimer, P. Kaatz, P. Günter, *Organic Nonlinear Optical Materials; Advances in Nonlinear Optics*, Vol. *1*, Gordon and Breach, Langhorne, PA **1995**.

[2] a) H. S. Nalwa, T. Watanabe, S. Miyata, in *Nonlinear Optics of Organic Molecules and Polymers*, (Eds: H. S. Nalwa, S. Miyata), CRC Press, Boca Raton, FL **1997**, Ch. 4. b) L. Dalton, P. Sullivan, A. K. Y. Jen, in *Handbook of Photonics*, (Eds: M. C. Gupta, J. Ballato), CRC Press, Boca Raton, FL **2007**. c) D. S. Chemla, J. Zyss, in *Nonlinear Optical Properties of Organic Molecules and Crystals*, Vol. 1, Academic Press, New York **1987**.

[3] a) T. Kaino, B. Cai, K. Takayama, *Adv. Funct. Mater.* **2002**, *12*, 599. b) W. Geis, R. Sinta, W. Mowers, S. J. Deneault, F. Marchant, K. E. Krohn, S. J. Spector, D. R. Calawa, T. M. Lyszczarz, *Appl. Phys. Lett.* **2004**, *84*, 3729. c) L. Mutter, M. Koechlin, M. Jazbinsek, P. Günter, *Opt. Express* **2007**, *15*, 16828. d) L. Mutter, M. Jazbinsek, C. Herzog, P. Günter, *Opt. Express* **2008**, *16*, 731.

[4] a) B. Ferguson, X. C. Zhang, *Nat. Mater.* **2002**, *1*, 26. b) H. Hashimoto, H. Takahashi, T. Yamada, K. Kuroyanagi, T. Kobayashi, *J. Phys. Condens. Matter* **2001**, *13*, L529. c) J. J. Carey, R. T. Bailey, D. Pugh, J. N. Sherwood, F. R. Cruickshank, K. Wynne, *Appl. Phys. Lett.* **2002**, *81*, 4335. d) A. M. Sinyukov, M. R. Leahy, L. M. Hayden, M. Haller, J. Luo, A. K. Y. Jen, L. R. Dalton, *Appl. Phys. Lett.* **2004**, *85*, 5827. e) A. Nahata, D. H. Auston, C. Wu, J. T. Yardley, *Appl. Phys. Lett.* **1995**, *67*, 1358. f) K. Kuroyanagi, K. Yanagi, A. Sugita, H. Hashimoto, H. Takahashi, S. Aoshima, Y. Tsuchiya, *J. Appl. Phys.* **2006**, *100*, 043117. g) M. Tonouchi, *Nat. Photonics* **2007**, *1*, 97.

[5] a) A. Schneider, M. Neis, M. Stillhart, B. Ruiz, R. U. A. Khan, P. Günter, *J. Opt. Soc. Am. B* **2006**, *23*, 1822. b) A. Schneider, I. Biaggio, P. Günter, *Appl. Phys. Lett.* **2004**, *84*, 2229. c) A. Schneider, M. Stillhart, P. Günter, *Opt. Express* **2006**, *14*, 5376.

[6] a) G. R. Desiraju, *Acc. Chem. Res.* **2002**, *35*, 565. b) G. R. Desiraju, *Acc. Chem. Res.* **1996**, *29*, 441.

[7] a) S. Okada, A. Masaki, H. Matsuda, H. Nakanishi, M. Kato, R. Muramatsu, M. Otshuka, *Jpn. J. Appl. Phys.* **1990**, *29*, 1112. b) A. Carenco, J. Jerphagnon, A. Perigaud, *J. Chem. Phys.* **1977**, *66*, 3806. c) I. Liakatas, M. S. Wong, V. Gramlich, C. Bosshard, P. Günter, *Adv. Mater.* **1998**, *10*, 777.

[8] F Pan,, M. S. Wong, V. Gramlich, C. Bosshard, P. Günter, *J. Am. Chem. Soc.* **1996**, *118*, 6315.

[9] a) O. P. Kwon, B. Ruiz, A. Choubey, L. Mutter, A. Schneider, M. Jazbinsek, P. Günter, *Chem. Mater.* **2006**, *18*, 4049. b) A. Choubey, O. P. Kwon, M. Jazbinsek, P. Günter, *Cryst. Growth Des.* **2007**, *7*, 402. c) O. P. Kwon, S. J. Kwon, M. Stillhart, M. Jazbinsek, A. Schneider, V. Gramlich, P. Günter, *Cryst. Growth Des.* **2007**, *7*, 2517.

[10] S. J. Kwon, O. P. Kwon, J. I. Seo, M. Jazbinsek, L. Mutter, V. Gramlich, Y. S. Lee, H. Yun, P. Günter, *J. Phys. Chem. C.* **2008**, *112*, 7846.

[11] O. P. Kwon, S. J. Kwon, M. Jazbinsek, V. Gramlich, P. Günter, *Adv. Funct. Mater.* **2007**, *17*, 1750.

[12] a) R. Lemke, *Chem. Ber.* **1970**, *103*, 1894. b) R. Lemke, *Synthesis* **1974**, 359.

[13] T. Kolev, Z. Glavcheva, D. Yanchev, M. Schürmann, D. C. Kleb, H. Preut, P. Bleckmann, *Acta Crystallogr. Sect. E* **2001**, *57*, o561.

[14] S. Ermer, S. M. Lovejoy, D. S. Leung, H. Warren, C. R. Moylan, R. J. Twieg, *Chem. Mater.* **1997**, *9*, 1437.

[15] a) S. R. Marder, J. W. Perry, W. P. Schaefer, *Science* **1989**, *245*, 626. b) S. R. Marder, J. W. Perry, C. P. Yakymyshyn, *Chem. Mater.* **1994**, *6*, 1137. c) F. Pan, M. S. Wong, C. Bosshard, P. Günter, *Adv. Mater.* **1996**, *8*, 592. d) F. Pan, G. Knöpfle, C. Bosshard, S. Follonier, R. Spreiter, M. S. Wong, P. Günter, *Appl. Phys. Lett.* **1996**, *69*, 13.

[16] I. Liakatas, C. Cai, M. Bösch, M. Jager, C. Bosshard, P. Günter, C. Zhang, L. R. Dalton, *Appl. Phys. Lett.* **2000**, *76*, 1368.

[17] a) B. J. Coe, J. A. Harris, I. Asselberghs, K. Clays, G. Olbrechts, A. Persoons, J. T. Hupp, R. C. Johnson, S. J. Coles, M. B. Hursthouse, K. Nakatani, *Adv. Funct. Mater.* **2002**, *12*, 110. b) B. Ruiz, B. J. Coe, R. Gianotti, V. Gramlich, M. Jazbinsek, P. Günter, *Cryst EngComm* **2007**, *9*, 772.

[18] D. Rezzonico, S. J. Kwon, H. Figi, O. P. Kwon, M. Jazbinsek, P. Günter, *J. Chem. Phys.* **2008**, *128*, 124713.

[19] a) A. D. Becke, *J. Chem. Phys.* **1993**, *98*, 5648. b) J. P. Perdew, *Phys. Rev. B* **1986**, *33*, 8822.

[20] M. J. Frisch, G. W. Trucks, H. B. Schlegel, G. E. Scuseria, M. A. Robb, J. R. Cheeseman, J. A. Montgomery, Jr., T. Vreven, K. N. Kudin, J. C. Burant, J. M. Millam, S. S. Iyengar, J. Tomasi, V. Barone, B. Mennucci, M. Cossi, G. Scalmani, N. Rega, G. A. Petersson, H. Nakatsuji, M. Hada, M. Ehara, K. Toyota, R. Fukuda, J. Hasegawa, M. Ishida, T. Nakajima, Y. Honda, O. Kitao, H. Nakai, M. Klene, X. Li, J. E. Knox, H. P. Hratchian, J. B. Cross, V. Bakken, C. Adamo, J. Jaramillo, R. Gomperts, R. E. Stratmann, O. Yazyev, A. J. Austin, R. Cammi, C. Pomelli, J. W. Ochterski, P. Y. Ayala, K. Morokuma, G. A. Voth, P. Salvador, J. J. Dannenberg, V. G. Zakrzewski, S. Dapprich, A. D. Daniels, M. C. Strain, O. Farkas, D. K. Malick, A. D. Rabuck, K. Raghavachari, J. B. Foresman, J. V. Ortiz, Q. Cui, A. G. Baboul, S. Clifford, J. Cioslowski, B. B. Stefanov, G. Liu, A. Liashenko, P. Piskorz, I. Komaromi, R. L. Martin, D. J. Fox, T. Keith, M. A. Al-Laham, C. Y. Peng, A. Nanayakkara, M. Challacombe, P. M. W. Gill, B. Johnson, W. Chen, M. W. Wong, C. Gonzalez, J. A. Pople, *Gaussian 03*, Revision C.02, Gaussian, Inc, Wallingford, CT **2004**.

[21] K. Kurtz, T. T. Perry, *J. Appl. Phys.* **1968**, *39*, 3798.

[22] C. Hunziker, S. J. Kwon, H. Figi, F. Juvalta, O. P. Kwon, M. Jazbinsek, P. Günter, unpublished.
[23] M. Walther, K. Jensby, S. R. Keiding, H. Takahashi, H. Ito, *Opt. Lett.* **2000**, *25*, 911.
[24] G. Sheldrick, SHELXL-97. Program for the Refinement of Crystal Structures. University of Göttingen, Germany **1997**.
[25] C. Bosshard, G. Knöpfle, P. Prêtre, P. Günter, *J. Appl. Phys.* **1992**, *71*, 1594.
[26] R. C. Eckardt, H. Masuda, Y. X. Fan, R. L. Byer, *IEEE J. Quantum Electron.* **1990**, *26*, 922.
[27] a) J. L. Oudar, D. S. Chemla, *J. Chem. Phys.* **1977**, *66*, 2664. b) J. L. Oudar, *J. Chem. Phys.* **1977**, *67*, 446.